Dissipative Quantum Hall Effect in Graphene near the Dirac Point

Dmitry A. Abanin,[1] Kostya S. Novoselov,[2] Uli Zeitler,[3] Patrick A. Lee,[1] A. K. Geim,[2,†] and L. S. Levitov[1,*]

[1]*Department of Physics, Massachusetts Institute of Technology, 77 Massachusetts Ave, Cambridge, Massachusetts 02139, USA*
[2]*Department of Physics and Astronomy, University of Manchester, Manchester, M13 9PL, United Kingdom*
[3]*High Field Magnet Laboratory, IMM, Radboud University Nijmegen, 6525 ED Nijmegen, The Netherlands*
(Received 5 February 2007; published 11 May 2007)

We report on the unusual nature of the $\nu = 0$ state in the integer quantum Hall effect (QHE) in graphene and show that electron transport in this regime is dominated by counterpropagating edge states. Such states, intrinsic to massless Dirac quasiparticles, manifest themselves in a large longitudinal resistivity $\rho_{xx} \gtrsim h/e^2$, in striking contrast to ρ_{xx} behavior in the standard QHE. The $\nu = 0$ state in graphene is also predicted to exhibit pronounced fluctuations in ρ_{xy} and ρ_{xx} and a smeared zero Hall plateau in σ_{xy}, in agreement with experiment. The existence of gapless edge states puts stringent constraints on possible theoretical models of the $\nu = 0$ state.

The electronic properties of graphene [1], especially the anomalous integer quantum Hall effect (QHE) [2,3], continue to attract significant interest. Graphene features QHE plateaus at half-integer values of $\sigma_{xy} = (\pm 1/2, \pm 3/2, \ldots) 4e^2/h$ where the factor 4 accounts for double valley and double spin degeneracy. The "half-integer" QHE is now well understood as arising due to unusual charge carriers in graphene, which mimic massless relativistic Dirac particles. Recent theoretical efforts have focused on the properties of spin- and valley-split QHE at low filling factors [4–9] and fractional QHE [10]. Novel states with dynamically generated excitonlike gap were conjectured near the Dirac point [11–13]. However, experiments in ultrahigh magnetic fields [14] have so far revealed only additional integer plateaus at $\nu = 0$, ± 1 and ± 4, which were attributed to valley and spin splitting.

The most intriguing QHE state is arguably that observed at $\nu = 0$. Being intrinsically particle-hole symmetric, it has no analog in semiconductor-based QHE systems. Interestingly, while it exhibits a steplike feature in σ_{xy}, the experimentally measured longitudinal and Hall resistance [14] (ρ_{xx} and ρ_{xy}) display neither a clear quantized plateau nor a zero-resistance state, the hallmarks of the conventional QHE. This unusual behavior was attributed to sample inhomogeneity [14] and remains unexplained. In this Letter, we show that such behavior near the Dirac point is in fact intrinsic to Dirac fermions in graphene and indicates an opening of a spin gap in the energy spectrum [4]. The gap leads to counter-circulating edge states carrying opposite spin [4,5] which result in interesting and rather bizarre properties of this QHE state. In particular, even in the complete absence of bulk conductivity, this state has a nonzero $\rho_{xx} \gtrsim h/2e^2$ (i.e., the QHE state is dissipative) whereby ρ_{xy} can change its sign as a function of density without exhibiting a plateau.

We start by reviewing the experimental situation near $\nu = 0$. Our graphene devices were fabricated as described in Ref. [1] and fully characterized in fields B up to 12 T at temperatures down to 1 K, revealing the behavior characteristic of single-layer graphene [2]. Several devices were then investigated in B up to 30 T, where, besides the standard half-integer QHE sequence, the $\nu = 0$ plateau becomes clearly visible as an additional step in σ_{xy} (Fig. 1). We note, however, that the step is not completely flat, and there is no clear zero-resistance plateau in ρ_{xy}. Instead, ρ_{xy} exhibits a fluctuating feature away from zero which seems trying to develop in a plateau [Fig. 1(b)]. [In some devices ρ_{xy} passed through zero in a smooth way without fluctuations.] Moreover, ρ_{xx} does not exhibit a zero-resistance state either. Instead, it has a pronounced peak near zero ν which does not split in any field. The value at the peak grows from $\rho_{xx} \approx h/4e^2$ in zero B to $\rho_{xx} > 45$ kΩ at 30 T [see inset of Fig. 1(b)].

The absence of both hallmarks of the conventional QHE could cast doubt on the relation between the observed extra step in σ_{xy} and an additional QHE plateau. However, the described high-field behavior near $\nu = 0$ was found to be universal (reproducible for different samples, measurement geometries and magnetic fields above 20 T). It is also in agreement with that reported in Ref. [14]. Moreover, one can generally argue that the QHE at $\nu = 0$ cannot possibly exhibit the usual hallmarks. Indeed, ρ_{xx} cannot exhibit a zero-resistance state simultaneously with ρ_{xy} passing through zero due to the carrier-type change because zero in both ρ_{xy} and ρ_{xx} would indicate a dissipationless (superconducting) state.

To analyze the anomalous behavior of the high-field QHE, we note that all microscopic models near the Dirac point can be broadly classified in two groups, QH metal and QH insulator, as illustrated in Fig. 2. Transport properties in these two cases are very different. The QH insulator [Fig. 2(b)] is characterized by strongly temperature dependent resistivity diverging at low T. The metallic T dependence observed at $\nu = 0$ clearly rules out this scenario. In the QH metal [Fig. 2(a)], a pair of gapless edge excitations [Fig. 2(a)] provides dominant contribution to
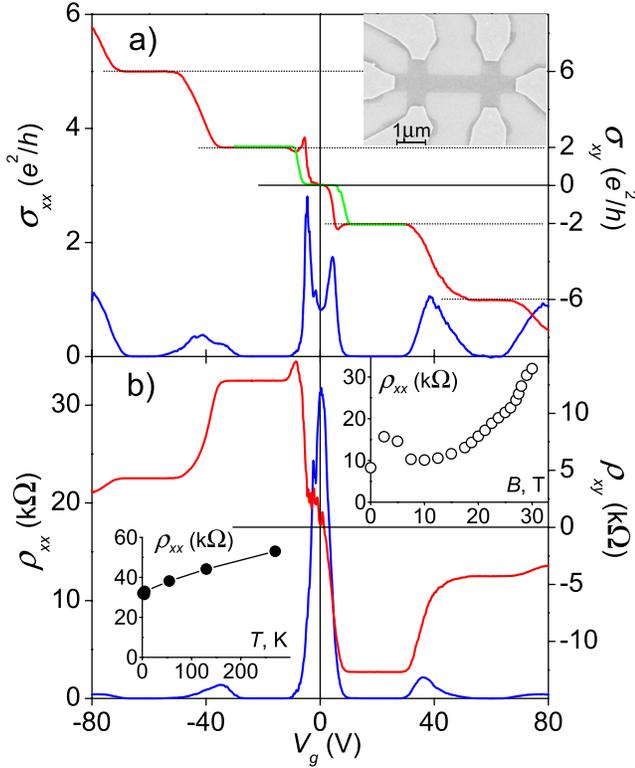
FIG. 1 (color online).   Longitudinal and Hall conductivities σ_{xx} and σ_{xy} (a) calculated from ρ_{xx} and ρ_{xy} measured at 4 K and $B = 30$ T (b). The $\nu = 0$ plateau in σ_{xy} and the double-peak structure in σ_{xx} arise mostly from strong density dependence of ρ_{xx} peak (green trace shows σ_{xy} for another sample). The upper inset shows one of our devices. The lower insets show temperature and magnetic field dependence of ρ_{xx} near $\nu = 0$. Note the metallic temperature dependence of ρ_{xx}.

σ_{xx}, while transport in the bulk is suppressed by an energy gap. Such a *dissipative QHE state* will have $\sigma_{xx} \sim e^2/h \gg \sigma_{xy}$, i.e., nominally small Hall angle and apparently no QHE. The roles of bulk and edge transport here effectively interchange: The longitudinal response is due to edge states, while the transverse response is determined mainly by the bulk properties.
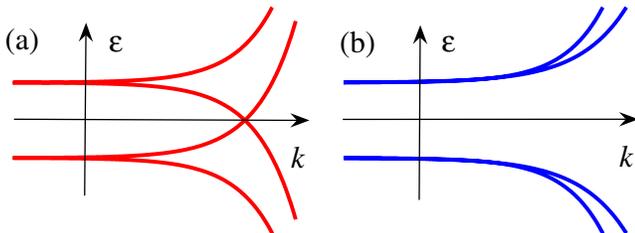

FIG. 2 (color online).   Excitation dispersion in $\nu = 0$ QH state with and without gapless chiral edge modes, (a) and (b) respectively. Case (a) is realized in spin-polarized $\nu = 0$ state [4], while case (b) occurs when symmetry is incompatible with gapless modes, for example, in valley-polarized $\nu = 0$ state conjectured in Ref. [14]. In the latter state a gap opens at branch crossing due to valley mixing at the sample boundary.

From a general symmetry viewpoint advanced in Ref. [15] the existence of counter-circulating gapless excitations is controled by Z_2 invariants, protecting the spectrum from gap opening at branch crossing. In the spin-polarized QHE state [4] this invariant is given by σ_z. While for other $\nu = 0$ QHE states [11–13] such invariants are not known, any viable theoretical model must present a mechanism to generate gapless edge states.

The metallic temperature dependence indicates strong dephasing that prevents onset of localization. To account for this observation, we suppose that the mean free path along the edge is sufficiently large, such that local equilibrium in the energy distribution is reached in between backscattering events. For that, the rate of inelastic processes must exceed the elastic backscattering rate: $\nu_{\text{inel}} \gg \nu_{\text{el}}$. This situation occurs naturally in the Zeeman-split QHE state [4], since backscattering between chiral modes carrying opposite spins is controlled by spin-orbital coupling which is small in graphene.

In the dephased regime, the chiral channels are described by local chemical potentials, $\varphi_{1,2}(x)$, whose deviation from equilibrium is related to currents:

$$ I_1 = \frac{e^2}{h}\varphi_1, \qquad I_2 = \frac{e^2}{h}\varphi_2, \qquad I = I_1 - I_2, \quad (1) $$

where I is the total current *on one edge*. In the absence of backscattering between the channels the currents $I_{1,2}$ are conserved. In this case, since the potentials $\varphi_{1,2}$ are constant along the edge, transport is locally nondissipative, similar to the usual QHE [16].

The origin of longitudinal resistance in this ideal case can be traced to the behavior in the contact regions. [Note the resemblance of each edge in Fig. 3(a) with two-probe measurement geometry for the standard QHE.] We adopt the model of termal reservoirs [17] which assumes full mixing of electron spin states within Ohmic contacts [see Fig. 3(b)]. With currents I_1, I_2 flowing into the contact, and equal currents $I_{1,2}^{\text{(out)}} = \frac{1}{2}(I_1 + I_2)$ flowing out, the potential of the probe is $V_{\text{probe}} = \frac{h}{e^2}I_{1,2}^{\text{(out)}}$. Crucially, using Eq. (1), there is a potential drop across the contact,
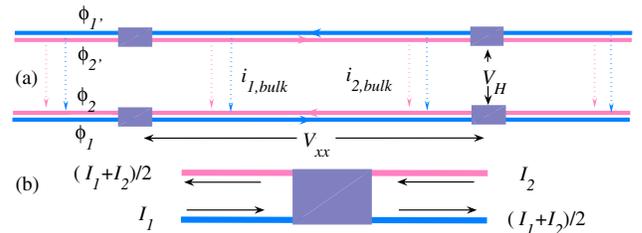

FIG. 3 (color online).   (a) Schematic of transport in a Hall bar with voltage probes. Chiral edge states carrying opposite spin, Eqs. (3), are denoted by red and blue. Transport through the bulk is indicated by dotted lines. (b) Voltage probe in a full spin mixing regime [17] measures $V_{\text{probe}} = \frac{h}{2e^2}(I_1 + I_2)$. Note finite voltage drop across the probe, Eq. (2).

$$\Delta\varphi = \frac{h}{2e^2}(I_1 - I_2), \qquad (2)$$

equally for φ_1 and φ_2. The voltage between two contacts positioned at the same edge [see Fig. 3(a)] is equal to $V_{xx} = \frac{h}{e^2}I$, which gives a universal resistance value [4]. This is in contrast with the usual QHE where there is no voltage drop between adjacent potential probes [16,17].

The longitudinal resistance increases and becomes nonuniversal in the presence of backscattering. It can be described by transport equations for charge density

$$\partial_t n_1 + \partial_x \varphi_1 = \gamma(\varphi_2 - \varphi_1),$$
$$\partial_t n_2 - \partial_x \varphi_2 = \gamma(\varphi_1 - \varphi_2), \qquad n_i = \nu_i \varphi_i, \qquad (3)$$

where γ^{-1} is the mean free path for $1d$ backscattering between modes 1 and 2, and $\nu_{1,2}$ are compressibilities of the modes 1 and 2. In a stationary state, Eqs. (3) have an integral $\tilde{I} = \varphi_1 - \varphi_2$ which expresses conservation of current $I = \frac{e^2}{h}\tilde{I}$. The general solution in the stationary current-carrying state is $\varphi_{1,2}(x) = \varphi_{1,2}^{(0)} - \gamma x \tilde{I}$.

For the Hall bar geometry shown in Fig. 3(a), taking into account the contribution of voltage drop across contacts, Eq. (2), we find the voltage along the edge $V_{xx} = (\gamma L + 1)\tilde{I}$, where L is the distance between the contacts. In the absence of transport through the bulk, if both edges carry the same current, the longitudinal resistance is

$$R_{xx} = (\gamma L + 1)\frac{h}{2e^2}, \qquad \rho_{xx} = (w/L)R_{xx}, \qquad (4)$$

with w/L the aspect ratio. From ρ_{xx} peak value (Fig. 1) we estimate $\gamma w \approx 2.5$, which gives the backscattering mean free path of 0.4 μm. The metallic T dependence of ρ_{xx} signals an increase of scattering with T [Fig. 1(b) inset]. Similarly, ρ_{xx} growing with B is explained by enhancement in scattering due to electron wave function pushed at high B towards the disordered boundary.

An important consequence of the $1d$ edge transport is the enhancement of fluctuations caused by position dependence of the scattering rate $\gamma(x)$. Solving for the potentials at the edge,

$$\varphi_{1,2}(x) = \varphi_{1,2}^{(0)} - \tilde{I}\int_0^x \gamma(y)dy, \qquad (5)$$

we see that the fluctuations in the longitudinal resistance scale as a square root of separation between the contacts:

$$\delta V_{xx} = \tilde{I}\int_{x_1}^{x_2} \delta\gamma(y)dy, \qquad \delta R_{xx} \sim (h/e^2)\sqrt{L/a},$$

where $a \gtrsim \gamma^{-1}$ is a microscopic length which depends on the details of spatial correlation of $\gamma(x)$. Similar effect leads to fluctuations of the Hall voltage about zero average value at $\nu = 0$. Treating the fluctuations of the potential at each edge, Eq. (5), as independent, we estimate $\delta R_{xy} \sim (h/e^2)\sqrt{L/a}$, where L is the bar length.

These fluctuations manifest themselves in noisy features in the transport coefficients near $\nu = 0$, arising from the dependence of the effective scattering potential on electron density. Such features can indeed be seen in ρ_{xy} and ρ_{xx} around $\nu = 0$ [Fig. 1(b)]. As discussed below, away from $\nu = 0$ bulk transport can short-circuit the edge transport. This will lead to suppression of fluctuations in ρ_{xx} and ρ_{xy} away from $\nu = 0$, in agreement with the behavior of the fluctuations in Fig. 1(b).

Another source of asymmetry in voltage distribution on opposite sides of the Hall bar at zero ν is the potential drop on a contact, Eq. (2). This quantity can be nonuniversal for imperfect contacts, leading to finite transverse voltage. Such an effect can be seen in ρ_{xy} data in Fig. 1 near $\nu = 0$, where Hall effect in a pristine system would vanish.

To describe transport properties at finite densities around $\nu = 0$, we must account for transport in the bulk. This can be achieved by incorporating in Eq. (3) the terms describing the edge-to-bulk leakage:

$$\partial_x \varphi_1 = \gamma(\varphi_2 - \varphi_1) + g(\psi_1 - \varphi_1),$$
$$-\partial_x \varphi_2 = \gamma(\varphi_1 - \varphi_2) + g(\psi_2 - \varphi_2), \qquad (6)$$

where $\psi_{1,2}$ are the up- and down-spin electrochemical potentials in the bulk near the boundary. Transport in the interior of the bar is described by tensor current-field relations with the longitudinal and Hall conductivities $\sigma_{xx}^{(1,2)}$, $\sigma_{xy}^{(1,2)}$ for each spin component. Combined with current continuity, these relations yield $2d$ Laplace's equation for the quantities $\psi_{1,2}$, with boundary conditions supplied by current continuity at the boundary:

$$\sigma_{xx}^{(i)}\mathbf{n}.\nabla\psi_i + \sigma_{xy}^{(i)}\mathbf{n} \times \nabla\psi_i + g(\varphi_i - \psi_i) = 0, \qquad (7)$$

$i = 1, 2$, where $\mathbf{n}$ is a unit normal vector. [In Eq. (7) and below we use the units of $e^2/h = 1$.] To describe dc current, we seek a solution of Eqs. (6) on both edges of the bar with linear x dependence $\varphi_i(x) = \varphi_i^{(0)} - \mathcal{E}x$ which satisfies boundary conditions (7), where the functions $\psi_{1,2}$ have a similar linear dependence. The current is calculated from this solution as a sum of the contributions from the bulk and both edges. After elementary but somewhat tedious algebra we obtain a relation $I = 2\mathcal{E}/\tilde{\gamma}$, where

$$\frac{2}{\tilde{\gamma}} = \frac{4}{2\gamma + g} + \frac{w}{\rho_{xx}^{(1)}} + \frac{w}{\rho_{xx}^{(2)}} - \frac{\lambda w(\tilde{\sigma}_{xy}^{(1)}/\sigma_{xx}^{(1)} - \tilde{\sigma}_{xy}^{(2)}/\sigma_{xx}^{(2)})^2}{2 + \lambda/\sigma_{xx}^{(1)} + \lambda/\sigma_{xx}^{(2)}}, \qquad (8)$$

with w the bar width and $\lambda = wg\gamma/(2\gamma + g)$. The quantities $\tilde{\sigma}_{xy}^{(1,2)} = \sigma_{xy}^{(1,2)} \pm g/(2\gamma + g)$ represent the sum of the bulk and edge contributions to Hall conductivities, and $\rho_{xx}^{(1,2)}$ are defined as $\rho_{xx}^{(i)} = \sigma_{xx}^{(i)}/(\tilde{\sigma}_{xy}^{(i)2} + \sigma_{xx}^{(i)2})$. The quantity $\tilde{\gamma}$, Eq. (8), replaces γ in Eq. (4). At vanishing bulk conductivity, $\sigma_{xx}^{(1,2)} \to 0$, we recover $\tilde{\gamma} = \gamma$.

The Hall voltage can be calculated from this solution as $V_H = \frac{1}{2}(\varphi_1 + \varphi_2 - \varphi_{1'} - \varphi_{2'})$, where $\varphi_{i,i'}$ are variables at opposite edges. We obtain $V_H = \xi\mathcal{E}$, where
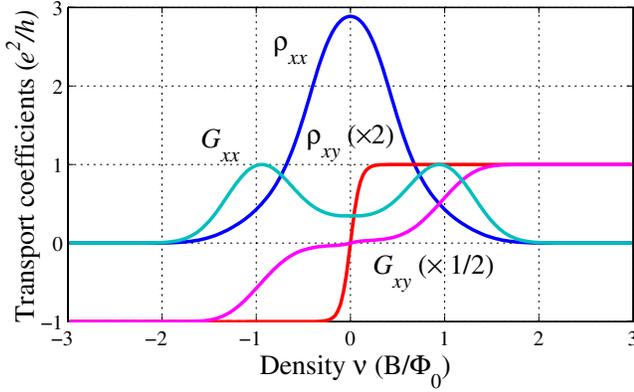
FIG. 4 (color online). Transport coefficients ρ_{xx}, ρ_{xy} and $G_{xx} = \rho_{xy}/(\rho_{xy}^2 + \rho_{xx}^2)$, $G_{xy} = \rho_{xy}/(\rho_{xy}^2 + \rho_{xx}^2)$ for a Hall bar (Fig. 3), obtained from the edge model (6) with account of bulk conductivity [Eqs. (10), (8), and (9), see text]. The edge transport shunted by the bulk conduction away from $\nu = 0$ results in the ρ_{xx} peak. Note the smooth behavior of ρ_{xy} at $\nu = 0$, a tilted plateau in G_{xy}, and a double-peak structure in G_{xx}.

$$\xi = 2w \frac{\tilde{\sigma}_{xy}^{(1)}(\lambda + \sigma_{xx}^{(2)}) + \tilde{\sigma}_{xy}^{(2)}(\lambda + \sigma_{xx}^{(1)})}{2\sigma_{xx}^{(1)}\sigma_{xx}^{(2)} + \lambda\sigma_{xx}^{(2)} + \lambda\sigma_{xx}^{(1)}}. \qquad (9)$$

This quantity vanishes at $\nu = 0$, since $\sigma_{xy}^{(1)} = -\sigma_{xy}^{(2)}$ and $\sigma_{xx}^{(1)} = \sigma_{xx}^{(2)}$ at this point due to particle-hole symmetry.

In Fig. 4 we illustrate the behavior of the longitudinal and transverse resistance, calculated from Eqs. (8) and (9), as

$$\rho_{xx} = w\tilde{\gamma}/2, \qquad \rho_{xy} = \xi\tilde{\gamma}/2, \qquad (10)$$

with $\gamma w = 6$, $gw = 1$ [the omitted contact term (2) is small for these parameters]. Conductivities $\sigma_{xx}^{(1,2)}$, $\sigma_{xy}^{(1,2)}$ are microscopic quantities, and their detailed dependence on the filling factor is beyond the scope of this paper. Here we model the conductivities $\sigma_{xx}^{(1,2)}$ by Gaussians centered at $\nu = \pm 1$, $\sigma_{xx}^{(1,2)}(\nu) = e^{-A(\nu \pm 1)^2}$, as appropriate for valley-degenerate Landau level, whereby $\sigma_{xy}^{(1,2)}$ is related to $\sigma_{xx}^{(1,2)}$ by the semicircle relation [18]: $\sigma_{xy}^{(1,2)}(\sigma_{xy}^{(1,2)} \mp 2) + (\sigma_{xx}^{(1,2)})^2 = 0$. In Fig. 4 we used $A = 5$: however, we note that none of the qualitative features depend on the details of the model.

Figure 4 reproduces many of the key features of the data shown in Fig. 1. The large peak in ρ_{xx} is due to edge transport near $\nu = 0$. The reduction in ρ_{xx} at finite ν is caused by the bulk conduction short circuiting the edge transport. The latter corresponds to the double-peak structure in G_{xx} in Fig. 4. We note that the part of G_{xx} between the peaks exceeds the superposition of two Gaussians which represent the bulk conductivity in our model. This excess in G_{xx} is the signature of the edge contribution. The transverse resistance ρ_{xy} is nonzero due to imbalance in $\sigma_{xy}^{(1,2)}$ for opposite spin polarizations away from the particle-hole symmetry point $\nu = 0$. Notably, ρ_{xy} does not show any plateau in the theoretical curve (Fig. 4), while G_{xy} calculated from ρ_{xy} and ρ_{xx} exhibits a plateaulike feature. This behavior is in agreement with experiment (Fig. 1 and Ref. [14]).

To conclude, QH transport in graphene at $\nu = 0$ indicates presence of counter-circulating edge states dominating the longitudinal resistivity whereas the Hall resistivity is governed by bulk propeties. Our model explains the observed behavior of transport coefficients, in particular, the peak in ρ_{xx} and its field and temperature dependence, lending strong support to the chiral spin-polarized edge picture of the $\nu = 0$ state.

*Electronic address: levitov@mit.edu
†Electronic address: geim@man.ac.uk

[1] K. S. Novoselov *et al.*, Science **306**, 666 (2004); Proc. Natl. Acad. Sci. U.S.A. **102**, 10 451 (2005).
[2] K. S. Novoselov *et al.*, Nature (London) **438**, 197 (2005).
[3] Y. Zhang, Y.-W. Tan, H. L. Stormer, and P. Kim, Nature (London) **438**, 201 (2005).
[4] D. A. Abanin, P. A. Lee, and L. S. Levitov, Phys. Rev. Lett. **96**, 176803 (2006).
[5] H. A. Fertig and L. Brey, Phys. Rev. Lett. **97**, 116805 (2006).
[6] K. Nomura and A. H. MacDonald, Phys. Rev. Lett. **96**, 256602 (2006).
[7] J. Alicea and M. P. A. Fisher, Phys. Rev. B **74**, 075422 (2006).
[8] M. O. Goerbig, R. Moessner, and B. Doucot, Phys. Rev. B **74**, 161407 (2006).
[9] D. A. Abanin, P. A. Lee, and L. S. Levitov, Phys. Rev. Lett. **98**, 156801 (2007).
[10] V. M. Apalkov and T. Chakraborty, Phys. Rev. Lett. **97**, 126801 (2006).
[11] V. P. Gusynin, V. A. Miransky, and I. A. Shovkovy, Phys. Rev. Lett. **73**, 3499 (1994); V. P. Gusynin *et al.*, Phys. Rev. B **74**, 195429 (2006).
[12] D. V. Khveshchenko, Phys. Rev. Lett. **87**, 206401 (2001); **87**, 246802 (2001).
[13] J.-N. Fuchs and P. Lederer, Phys. Rev. Lett. **98**, 016803 (2007).
[14] Y. Zhang *et al.*, Phys. Rev. Lett. **96**, 136806 (2006).
[15] L. Fu and C. L. Kane, Phys. Rev. B **74**, 195312 (2006); C. L. Kane and E. J. Mele, Phys. Rev. Lett. **95**, 226801 (2005).
[16] B. I. Halperin, Phys. Rev. B **25**, 2185 (1982).
[17] M. Büttiker, Phys. Rev. B **38**, 9375 (1988).
[18] A. M. Dykhne and I. M. Ruzin, Phys. Rev. B **50**, 2369 (1994); S. S. Murzin, M. Weiss, A. G. Jansen, and K. Eberl, Phys. Rev. B **66**, 233314 (2002).